Regular Article

NMR studies of benzene mobility in metal-organic framework MOF-5

S. Hertel[1], M. Wehring[1], S. Amirjalayer[2], M. Gratz[1], J. Lincke[3], H. Krautscheid[3], R. Schmid[2], and F. Stallmach[1,a]

[1] Fakultät für Physik und Geowissenschaften, Universität Leipzig, Linnéstrasse 5, 04103 Leipzig, Germany
[2] Lehrstuhl für Anorganische Chemie II, Ruhr-Universität Bochum, 44780 Bochum, Germany
[3] Fakultät für Chemie und Mineralogie, Universität Leipzig, Johannisallee 29, 04103 Leipzig, Germany

Abstract. The concentration and temperature dependence of the self-diffusion of benzene adsorbed in the metal-organic framework MOF-5 (IRMOF-1) is studied by pulsed field gradient (PFG) NMR spectroscopy. When increasing the loading from 10 to 20 molecules per unit cell of MOF-5, the experimental diffusion data drop by a factor of about 3 while current molecular dynamic (MD) simulations predict slightly increasing diffusion coefficients for this range of loadings. The observation is rationalized using the recently predicted clustering of adsorbate molecules in microporous systems for temperatures well below the adsorbate critical temperature. Necessary improvements of molecular simulation models for predicting diffusivities under such conditions are discussed.

1 Introduction

Porous coordination polymers so-called metal-organic frameworks (MOFs) are a relatively new class of crystalline microporous materials [1–5]. Generally, they consist of organic linker molecules and metal coordination centers, which form an ordered three-dimensional nanoporous network. The variety of possible linkers and coordination centers results in a large variety of matrix and pore space properties, making MOFs interesting for fundamental research of host-guest interactions as well as applications, e.g., in the fields of sensor design, gas storage, separation and catalysis, respectively [6–11].

Knowledge and prediction of the interactions of small molecules in the pore space of MOFs is important for many of these potential applications. With this respect, diffusion studies in such MOFs represent a challenging field for theoretical and experimental studies. Meanwhile there exist a large number of computer simulations (see, for example, Refs. [12–15]) and a few experimental techniques, such as interference and infrared microscopy [16–18], quasi-elastic neutron scattering (QENS) [19–21] and pulsed field gradient (PFG) NMR [22,23], which allow one to determine guest diffusion in MOFs under non-equilibrium and equilibrium conditions, respectively.

Comparisons between molecular simulations and experimental measurements of diffusion in MOFs are performed to learn, how molecules interact with the internal surface of the MOFs and how diffusion proceeds in the micropores. Simultaneously, they may allow screening of

materials for certain applications [7,8] as well as the test and the improvement of both, simulation models and experimental setups.

For example, while the results of experimental NMR studies and of MD simulations for self-diffusion of hydrocarbons in the MOF $Cu_2(BTC)_3$ agree for the activation energy, the absolute values of the experimental diffusivities are found to be somewhat lower and deviate in the prediction of the loading dependence compared to the MD simulations [23]. Chmelik et al. [17] measured the diffusion of butanes in the same MOF by IR microscopy and found agreeing trends in the loading dependencies of the Maxwell-Stefan diffusivities obtained from the experimental data and from molecular simulations. Salles et al. [20,21] compared QENS data and MD simulations for hydrogen diffusion in MIL-47 and MIL-53 [20] and for carbon dioxide diffusion in MIL-47 [21]. The authors found that force field parameters in the molecular simulations had to be adjusted to describe dynamic and thermodynamic properties of the hydrogen/MIL system. For carbon dioxide adsorbed at MIL-47(V) they found an unusual sharp increase in transport diffusivity at small loadings whereas the self-diffusivity decreased with increasing loading. From this observation, it was concluded that carbon dioxide does not behave like an ideal gas in this MOF. Finally, very recent molecular simulations by Krishna and van Baten [15] predict that in porous systems with sufficiently large micropores, the concentration dependence of the transport diffusion of adsorbate molecules changes for subcritical temperatures. For the system carbon dioxide in MOF-5 (the same as IRMOF-1

a e-mail: stallmac@physik.uni-leipzig.de

[1]), the authors conclude that at sufficiently high concentrations below the critical temperature carbon dioxide forms clusters. They also found that these clusters diffuse significantly slower through the pore space than the single molecules.

The aim of this contribution is to investigate the concentration and temperature dependence of self-diffusion of benzene in MOF-5 by the PFG NMR spin-echo technique [22] and by diffusion-relaxation correlation spectroscopy (DRCOSY) [24,25]. In recent work, we found an agreement between the results of PFG NMR [26] and MD simulations [13] at 298 K at a relatively low loading of six benzene molecules per unit cell of MOF-5. Later MD simulations predicted at 298 K a slightly increasing diffusivity for loadings up to about 32 molecules per unit cell which then falls off at higher loadings [27]. These results have not yet been verified by experimental studies. On the other hand at all temperatures accessible by current PFG NMR experiments and MD simulations, the system benzene at MOF-5 is well below the critical temperature of benzene, which according to the approach of Krishna and van Baten [15] might be in the condition where favorable adsorbate-adsorbate interactions lead to clustering of the benzene molecules. Thus, an influence of such clustering on self-diffusion might be expected as well.

2 Materials and methods

2.1 MOF-5 framework and self-diffusion

Synthesis and characterization of the porous crystalline coordination polymer MOF-5 was first reported by Li et al. [28]. Macroscopically, MOF-5 forms crystals with a density of $0.59 \, \text{g cm}^{-3}$ and a porosity of about 55%. 1,4-Benzenedicarboxylate (BDC) anions are linking regular Zn_4O tetrahedra forming a cubic 3D structure. The structure of the MOF-5 unit cell is shown in Figure 1. The phenyl rings of the BDC linkers and the nodes formed by the Zn_4O clusters may easily be identified. The unit cell itself contains two types of alternating cavities which differ slightly in the void space (larger A subcell and smaller B subcell with 1.5 nm and 1.1 nm diameter spheres fitting inside, respectively) and the accessibility of the metal centers for adsorbed molecules [27,28].

Inside microporous solids such as MOF-5, adsorbed molecules are persistently moving in the force field of the pore walls. Therefore, thermally activated motion inside this porous material can be considered as an activated process [29]. The temperature dependence of the self-diffusion coefficient D can be described accordingly by an Arrhenius type equation:

$$D(T) = D_0 \exp\left(-\frac{E_A}{RT}\right), \tag{1}$$

where D_0 denotes the diffusivity at infinite temperature (pre-exponential factor). E_A is the activation energy and R is the ideal gas constant.
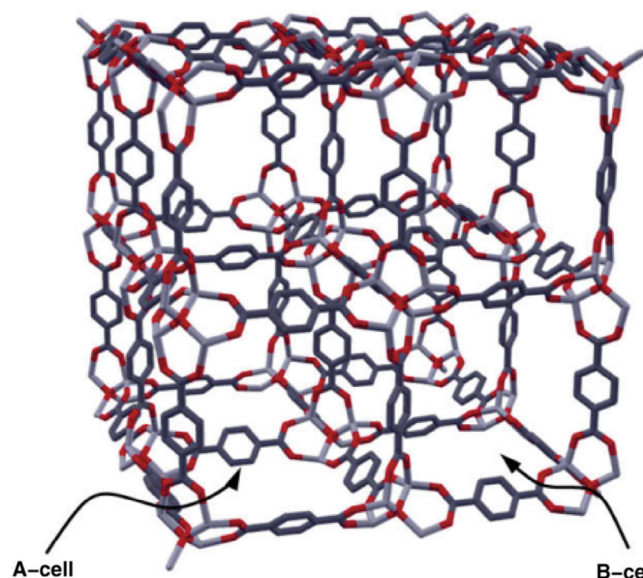

Fig. 1. (Color online) The unit cell of MOF-5 formed by four A- and four B-subcells.

At a given temperature, MD computer simulations as well as PFG NMR experiments allow one to study the time dependence of the mean square displacement $\langle r^2(t) \rangle$ of adsorbed molecules under equilibrium conditions. For both methods the relation to the self-diffusion coefficient is provided by the Einstein relation (three-dimensional case):

$$D = \langle r^2(t) \rangle / (6t). \tag{2}$$

Thus, comparison of both methods may yield insight into the mobilities and the interactions of adsorbed molecules in the MOF framework. However, the relevant time scales are different and of the order of nanoseconds for the MD simulations and of the order of a few tens of milliseconds for PFG NMR.

2.2 Pulsed field gradient NMR diffusion measurements

2.2.1 General relations and the stimulated spin-echo sequence

In the PFG NMR technique originally developed by Stejskal and Tanner [30] and Tanner [31] using the primary and the stimulated spin-echo sequences [32], the NMR spin-echo signal intensity is sensitive to the mean square displacement $\langle r^2(\Delta) \rangle$ during the time between the pair of pulsed field gradients ($t = \Delta$, see Fig. 2 and Eq. (2)). The spin-echo intensity $M(b)$ is measured as function of the so-called b-value, which depends on the gradient settings of the pulse sequence [22]. The b-value for a pair of rectangular gradient pulses is given by [22,30]

$$b = (\gamma G \delta)^2 \left(\Delta - \frac{1}{3}\delta\right), \tag{3}$$

where γ denotes the gyromagnetic ratio of the observed nucleus and all other physical quantities are defined using the example of the stimulated spin-echo sequence in
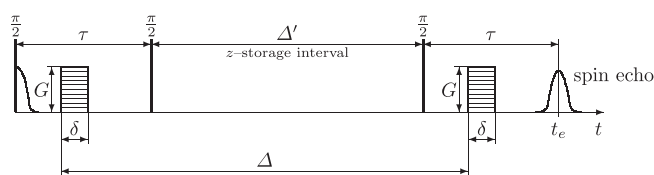
Fig. 2. Stimulated spin-echo NMR sequence for diffusion measurements with pulsed field gradients. For a given diffusion time Δ, the spin-echo NMR signal is weighted by transverse relaxation during the intervals τ and by longitudinal relaxation during the z-storage interval Δ' (see Eq. (4)). Further main experimental parameters are the strength G and the width δ of the pulsed field gradients.

Figure 2. The signal intensity for this stimulated spin-echo pulse sequence is given by [22,30,31]

$$\frac{M(b)}{M_0} = \exp(-Db)\exp\left(-\frac{2\tau}{T_2}\right)\exp\left(-\frac{\Delta'}{T_1}\right). \quad (4)$$

T_1 and T_2 are the longitudinal and transverse relaxation times of the spin system. τ and Δ' denote the storage intervals of magnetization in the x-y-plane and the z-direction, respectively. For PFG NMR experiments with all times fixed, but only the gradient strength G varied, relaxation leads to a constant attenuation factor and can be neglected in the analysis. If $M(0)$ is the reference without applied pulsed gradients, the self-diffusion coefficient D is obtained by analyzing the slope of the plot of $\ln(M(b)/M(0))$ versus b.

As can be seen in equation (4), relaxation is often the limiting factor for time-dependent self-diffusion studies using PFG NMR. In order to reduce the influence of transverse relaxation, the magnetization is stored in the longitudinal direction during the z-storage time interval Δ' (see Fig. 2). At time τ after beginning of the experiment, the second $\pi/2$ pulse stores the magnetization along the longitudinal axis. The magnetization is recalled by the third radiofrequency pulse and is rephased in a stimulated echo. During the z-storage period the magnetization is subject to the T_1 relaxation which is usually longer than the T_2 relaxation. Hence, the region of larger diffusion times Δ becomes available, enabling one to investigate slow self-diffusion in samples with short T_2 relaxation [22,31].

In multicomponent systems, where diffusion of the molecules carrying the nuclear spin under investigation may occur in different phases with different self-diffusion coefficients, the spin-echo attenuation is given by a superposition of corresponding exponential terms. In the case of two phases A and B with diffusion coefficients D_A and D_B, the spin-echo attenuation can be decomposed into a sum of two exponentials [22,33]:

$$\frac{M(b)}{M(0)} = p_A \exp(-D_A b) + p_B \exp(-D_B b), \quad (5)$$

where p_A and p_B are the population of both phases.

2.2.2 The 13-interval pulse sequence

In addition to the applied pulsed field gradients G there may also exist constant background gradients g. They are caused by inhomogeneities of the magnetic flux density of the polarizing NMR magnetic field (B_0). Especially in heterogeneous samples like beds of porous materials, background gradients are always present due to unavoidable magnetic susceptibility differences between the solid matrix material and the inter- and intracrystalline void space.

In order to avoid disturbing influences of such background gradients on the spin-echo attenuation, PFG NMR diffusion studies should be performed using the 13-interval pulse train plotted in Figure 3 [34]. This sequence suppresses cross terms between the externally applied pulsed field gradients and a constant background gradient g, if the pulsed gradients are centered in their τ-intervals, i.e., $\delta_1 = \delta_2$ in Figure 3. For this 13-interval sequence, the b-value controlling the diffusion-related spin-echo NMR signal attenuation in equations (4) and (5) is given by [22,34]

$$b = \gamma^2(2\delta)^2\left[\Delta' + \frac{3}{2}\tau - \frac{1}{6}\delta\right]G^2. \quad (6)$$

The transverse relaxation term in equation (4) changes to $\exp\left(-\frac{4\tau}{T_2} - \frac{4}{3}\gamma^2 g^2\tau^3 D\right)$, which is independent of the z-storage interval. Its influence on the spin-echo attenuation can be neglected if τ is kept constant and as short as possible during the 13-interval PFG NMR diffusion experiment.

2.2.3 The DRCOSY pulse sequence

In order to gain information about correlations between diffusivities and T_2 relaxation times, one may apply the so-called diffusion-relaxation correlation spectroscopy (DRCOSY) pulse sequence [24,25]. Figure 4 shows a typical DRCOSY pulse sequence. The first part consists of a stimulated spin-echo pulse sequence as described above. It is followed by a CPMG (Carr-Purcell-Meiboom-Gill) pulse sequence for T_2 measurement. At the beginning of the CPMG part, there is no new $\pi/2$ radiofrequency pulse
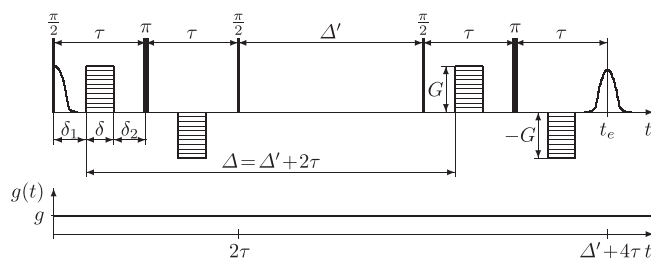

Fig. 3. 13-Interval pulse sequence with additional π rf-pulses and bipolar pulsed field gradients $G(t)$. A constantly acting background gradient $g(t)$ is indicated as well. For equal time intervals $\delta_1 = \delta_2$, disturbing effects of this background gradient are minimized. For more details, see references [22,34].
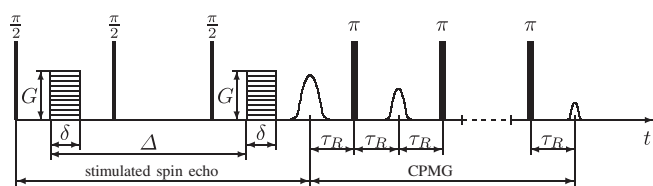
Fig. 4. DRCOSY pulse sequence consisting of two subsequences. The stimulated spin-echo subsequence with the pairs of pulsed field gradients allows to measure self-diffusion. It is followed by a CPMG pulse subsequence without new excitation pulse to record the transverse magnetization decay.

for excitation. Thus the CPMG pulse train (T_2-domain) is correlated to the residual NMR signal of the diffusion subsequence (D-domain).

Mathematically the normalized NMR signal is then described by [35, 36]

$$\frac{M(b,t)}{M(0)} = \iint dD\, dT_2\, p(D,T_2)$$
$$\times \exp\{-Db\} \exp\left\{-\frac{t}{T_2}\right\}. \quad (7)$$

This can be seen as $M(b,t)/M(0)$ being the two-dimensional Laplace transformation of the term $p(D,T_2)$. $p(D,T_2)$ represents the joint probability to find a spin with a certain D and T_2 contributing to the NMR signal. To obtain the desired distribution $p(D,T_2)$ one has to apply the inverse Laplace transformation $\mathcal{L}^{-1}$

$$p(D,T_2) = \mathcal{L}^{-1}\{M(b,t)\}. \quad (8)$$

In general discrete inverse Laplace transformations are mathematically ill-posed problems. Via regularization and by the approach of Venkataramanan et al. [35] and Song et al. [36] this problem became solvable by conventional desktop PCs.

3 Experimental

3.1 MOF-5 sample preparation and characterization

3.1.1 Synthesis

The synthesis of the MOF-5 samples is based on the approach of Eddaoudi et al. [2] and was modified to yield the desired crystal quality. Under continuous stirring, 0.665 g terephthalic acid and 3.14 g $Zn(NO_3)_2 \cdot 4H_2O$ were dissolved in 100 mL diethylformamide (DEF). The solution was kept at $T = 368\,K$ for 24 h and at $T = 378\,K$ for additional 5–10 h to achieve the necessary crystal size. During this time cubic crystals were precipitating, which were isolated by decanting the solvent. The crystals were washed several times with dimethylformamide (DMF) and with chloroform. Afterwards they were rinsed in benzene and dried at $T = 383\,K$ under dynamic vacuum for about 24 h. The obtained MOF-5 crystals have crystal sizes of 0.2–0.5 mm in diameter. To avoid contact with moisture and air, the crystals were stored under Argon atmosphere until preparation of samples for the NMR studies.

3.1.2 NMR sample preparation

Adsorption of benzene was done with about 90 mg of the MOF-5 samples, filled into a NMR sample tube of 7.5 mm outer diameter. In order to further remove residual solvents and gases from the pore structure, the samples were slowly heated under vacuum up to $T = 393\,K$, which was maintained for 48 h. Afterwards, the samples were cooled down to room temperature and immersed into liquid nitrogen. At $T = 77\,K$ the samples were exposed to volumetrically determined amounts of benzene gas and the appropriate amount of benzene froze in. Consecutively, the glass tubes were sealed via fusion of a capillary at the top of the NMR sample. A homogeneous distribution of benzene across the bed of MOF-5 in the sample tubes was ensured by storing the sealed samples for at least 24 h at room temperature before NMR measurements. The samples were loaded with 10, 20, 32 and 56 benzene molecules per unit cell of MOF-5. Throughout this report the samples are abbreviated by 10Bz, 20Bz, 32Bz and 56Bz, respectively.

3.1.3 X-ray structure analysis

The MOF-5 samples were checked for their crystal structure via X-ray powder diffraction (XRD). The first XRD was measured with the crystals as obtained from synthesis. The second XRD pattern was taken after the NMR diffusion studies with one of the benzene loaded samples (32Bz). Powder preparation was performed by opening the sample tubes, dashing the crystals to powder (short air exposure, partial desorption of the benzene) and filling the powder into a capillary (Hilgenberg capillaries glass No. 50, outer diameter 0.7 mm). The X-ray powder diffraction was carried out on a STOE STADI P diffractometer using Cu-K$_{\alpha 1}$ radiation ($\lambda = 154.060$ pm), a curved germanium (1 1 1) monochromator and a linear PSD as detector. STOE WinXPOW 2.15 (2006) was used to analyze the data and to calculate the theoretical pattern from the corresponding CIF which was obtained from the CCDC.

Figure 5 compares the measured XRD patterns of the two MOF-5 samples with the simulation from CIF. According to Hafizovic et al. [37], peak splitting and especially the intensity ratio between the peaks at 6.9° and at 9.6° indicate zinc hydroxide inclusions ($I_{6.9°}/I_{9.7°} < 1$) and interpenetrated MOF-5 crystal structures ($I_{6.9°}/I_{9.7°} \approx 1.33$), respectively. Both of our experimental XRD patterns do not show such splitting and such characteristic deviations from the simulated peak ratios ($I_{6.9°}/I_{9.7°} \approx 2$). The intensity ratio of the two most intense peaks as well as the positions of all other major peaks are found to be in agreement with the pattern obtained by the simulation from CIF (see Fig. 5). Thus, the presence of the expected MOF-5 crystal structure without substantial amounts of zinc hydroxide inclusions and interpenetrated frameworks could be confirmed by this XRD analysis. However, in the sample with benzene present in the pore space, the peak at 9.6° is clearly broadened compared to the simulated pattern. We assume that this is caused by
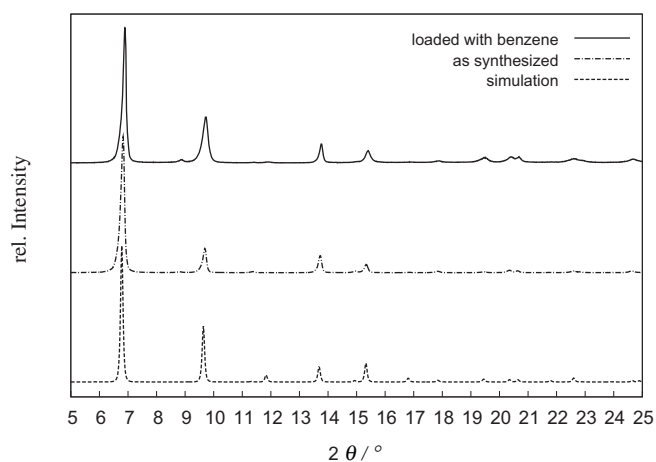
Fig. 5. X-ray powder diffraction pattern of MOF-5. Simulated from CIF (bottom), as synthesized (middle) and loaded with benzene (top).

a change in electron density due to the presence of mobile benzene molecules in the crystal structure.

3.1.4 Solid-state NMR analysis

For chemical analysis of the benzene/MOF-5 host-guest system ^{1}H MAS NMR spectra were measured on a Bruker Avance 400 NMR spectrometer. For these measurements, an additional sample was prepared in a glass tube with 2.9 mm outer diameter and loaded with benzene using the same procedure as described in Section 3.1.2. After sealing by fusion, this sample was inserted into a commercial MAS rotor of 4.0 mm outer diameter. For acquisition of the ^{1}H MAS NMR spectrum the sample was rotated with a frequency $\nu = 10$ kHz at a temperature of $T = 298$ K.

The ^{1}H MAS NMR spectrum of the benzene loaded MOF-5 sample shows three intense signals (see Fig. 6). The signal at about 7.2 ppm originates from the hydrogen nuclei at the adsorbed benzene molecules. This signal was used as internal chemical shift reference for this NMR spectrum. Obviously, the mobility of the adsorbed benzene molecules is still high enough to effectively average dipole-dipole interaction leading to the observed narrow NMR line. The much broader peak at 8.8 ppm comes from the much less mobile hydrogen atoms attached to the phenyl rings of the MOF-5 framework. In the static (no MAS) NMR diffusion studies, these hydrogen atoms do not contribute to the NMR signal due to their short solid-like transverse relaxation time. The broad but much smaller peak centered at about 2.1 ppm is typical for hydrogen atoms in aliphatic compounds of reduced mobility. Considering the MOF-5 synthesis procedure, it is most likely that it originates from protons in the ethyl groups of residual DEF solvent molecules which could not be removed after synthesis. Unfortunately, we were not able to resolve the expected three hydrogen resonances from the DEF as demonstrated by Loiseau et al. [38] for structural DEF molecules in an MOF-5 similar open-framework zinc terephthalate. Especially the ^{1}H resonance of the aldehyde
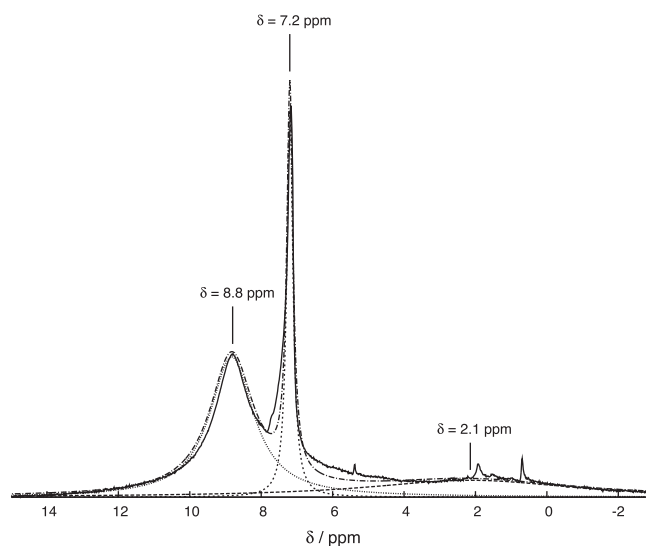

Fig. 6. ^{1}H MAS NMR spectrum of a benzene loaded MOF-5 sample. The narrow peak at about 7.2 ppm was assigned to the adsorbed benzene. The peak at about 8.8 ppm originates from the phenyl groups of the MOF-5 framework. The broad peak at 2.1 ppm represents most likely the superposition of the ^{1}H resonances of the CH_2-CH_3 groups of residual, immobile DEF (solvent) molecules. Not assigned small narrow resonance lines are from hydroxyl groups on the glass surface of the NMR sample tube.

function of the DEF molecule at about 8 ppm is not resolved and covered by the broad resonance of the lattice phenyl groups. However, the presence of DEF molecules is also visible in FTIR spectra of these MOF-5 samples (data not shown).

In order to estimate the amount of such residual DEF molecules in our sample, the observed ^{1}H MAS NMR spectrum was fitted to Lorentz lines at the three above given chemical shift positions (see lines in Fig. 6) and the obtained peak areas were compared. The ratio of the peak areas is 100:39:39 for the superposition of the ^{1}H phenyl resonances of the MOF-5 lattice (96 H-atoms per unit cell) and the aldehyde function of DEF molecules (1 H-atom per molecule), the adsorbed benzene (6 H-atoms per molecule) and the ethyl groups of residual DEF molecules (10 H-atoms per molecule), respectively. From these data we estimate that we have less than about 4 DEF molecules and 6–7 benzene molecules per MOF-5 unit cell in this sample. Since one unit cell consists of 4 A and 4 B subcells (compare Fig. 1), this NMR result means that – on average – about every second subcell is occupied by a DEF molecule not removed by sample preparation.

3.2 PFG NMR diffusion parameters

PFG NMR diffusion measurements including DRCOSY experiments were performed on the home-built NMR spectrometer FEGRIS NT [39] operating at 125 MHz ^{1}H resonance frequency. The NMR studies were conducted at selected temperatures in the range of 213 K $\leq T \leq$ 328 K.

The sample temperature was controlled by a stream of air (above room temperature) or nitrogen (below room temperature) with an accuracy of $\pm 1\,\mathrm{K}$.

Typical parameters for the ^{1}H PFG NMR diffusion studies with the stimulated spin-echo sequence were $\tau = 2\,\mathrm{ms}$ and variable diffusion times $5\,\mathrm{ms} \leq \Delta \leq 160\,\mathrm{ms}$. The pulsed field gradient width was $\delta = 300\,\mu\mathrm{s}$. For the 13-interval sequence the parameters were $2\tau = 2\,\mathrm{ms}$, which ensured the same transverse relaxation time weighting as in the stimulated spin-echo sequence, and diffusion times $5\,\mathrm{ms} \leq \Delta \leq 40\,\mathrm{ms}$. Spin-echo attenuations were measured by increasing the pulsed field gradient strength G from 0 up to a maximum value of $29\,\mathrm{T\,m}^{-1}$.

Typical parameters for the DRCOSY sequence were $\tau = 1\,\mathrm{ms}$, pulsed field gradient width $\delta = 300\,\mu\mathrm{s}$, variable diffusion times $10\,\mathrm{ms} \leq \Delta \leq 40\,\mathrm{ms}$ and for the CPMG part $\tau_R = 500\,\mu\mathrm{s}$.

4 Results and discussion

The diffusion measurements were carried out with the benzene loaded MOF-5 samples described in Section 3.1.2. For example, Figure 7 illustrates typical PFG NMR spin-echo attenuations obtained using the stimulated spin echo and the 13-interval pulse sequence at two different temperatures. In the case of single component diffusion in a homogeneous medium, one would expect a single-exponential decay of the data as function of the b-value, which does not depend on the pulse sequence applied. The slope of this decay would yield the desired self-diffusion coefficient. However, in the benzene loaded MOF-5 sample plotted in Figure 7, one observes for both pulse sequences clear deviations from a single-exponential signal decay and the 13-interval sequence yields a lower attenuation compared to the stimulated spin-echo data. Additionally, while the measurements with the stimulated spin echo showed a dependence on observation time at high benzene loadings (data not shown), we did not detect any dependence of the spin-echo attenuations on the observation times for $10\,\mathrm{ms} \leq \Delta \leq 40\,\mathrm{ms}$ when using the 13-interval sequence.

In the heterogeneous bed of MOF-5 crystals, magnetic susceptibility differences between the inter- and intracrystalline space will induce static background gradients. Since the 13-interval sequence is known to cancel disturbing influences of cross terms between the externally applied pulsed field gradients and such background gradients, we assume that only the flatter and diffusion time-independent spin-echo attenuations observed with the 13-interval sequence are representative for the self-diffusion of the adsorbed benzene molecules. Consequently, we concentrated on the interpretation of the experimental data obtained with the 13-interval sequence.

Figure 8 plots the spin-echo attenuations obtained by the 13-interval sequence for the sample loaded with 32 benzene molecules per unit cell for different temperatures. The deviations from single-exponential decay are obvious for all temperatures. The data were analyzed by a bi-exponential function (see Eq. (5)) representing a two component diffusion process. Table 1 lists the results of
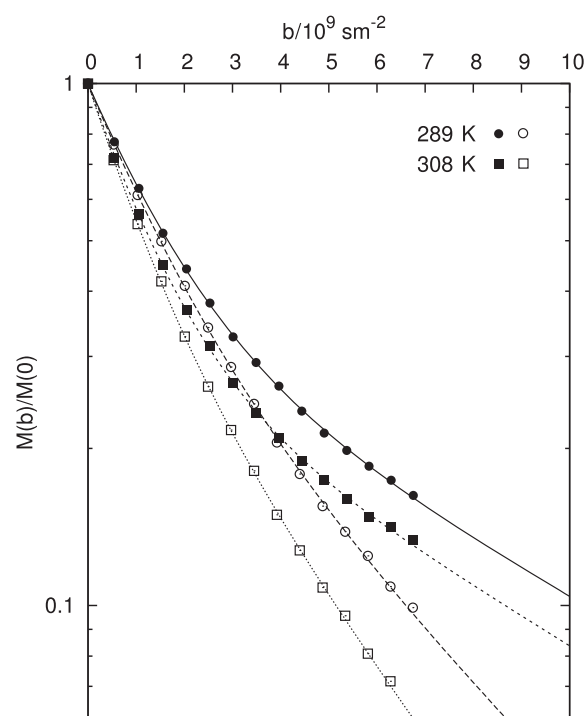

Fig. 7. Comparison of the PFG NMR spin-echo attenuation curves obtained by the stimulated echo (open symbols) and 13-interval sequence (full symbols) for benzene adsorbed at MOF-5 (32Bz) at temperatures of 298 K and 308 K. The diffusion time was $\Delta = 20\,\mathrm{ms}$.
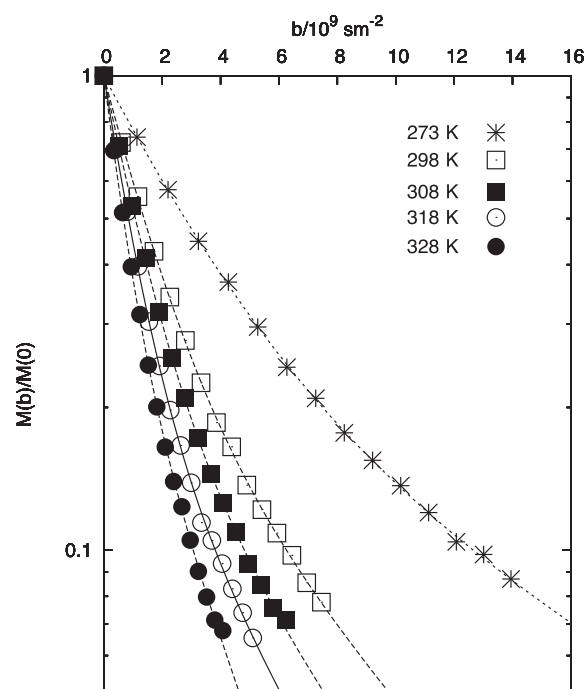

Fig. 8. 13-Interval sequence PFG NMR spin-echo attenuation curves for benzene adsorbed in MOF-5 (32Bz) observed at different temperatures. The diffusion time was $\Delta = 20\,\mathrm{ms}$. The lines represent the bi-exponential fits with the parameters given in Table 1.

Table 1. Temperature dependence of the self-diffusion coefficients of benzene in MOF-5 (32 molecules per unit cell) obtained by a bi-exponential fit (Eq. (5)) of the spin-echo attenuation curves from Figure 8. Fast component D_A with relative weight p_A and slow component D_B (relative weight $1-p_A$, not given).

T [K]	p_A	D_A [$10^{-10}\,\mathrm{m}^2\,\mathrm{s}^{-1}$]	D_B [$10^{-10}\,\mathrm{m}^2\,\mathrm{s}^{-1}$]
273	0.73	3.54	0.92
298	0.75	7.07	1.79
308	0.77	8.79	2.20
318	0.77	11.30	2.74
328	0.70	15.10	4.16

this bi-exponential fit. At all temperatures, the two components with different self-diffusion coefficients (D_A and D_B) have relative weights of about 70% for the fast component (A) and 30% for the slow component (B). With increasing temperature, the self-diffusion coefficients increase from $3.54 \times 10^{-10}\,\mathrm{m}^2\,\mathrm{s}^{-1}$ to $1.51 \times 10^{-9}\,\mathrm{m}^2\,\mathrm{s}^{-1}$ for the faster component and from $0.92 \times 10^{-10}\,\mathrm{m}^2\,\mathrm{s}^{-1}$ to $4.16 \times 10^{-10}\,\mathrm{m}^2\,\mathrm{s}^{-1}$ for the slower component. Independent of temperature, fast and slow diffusion coefficients are found to differ approximately by a factor of 3.5.

The diffusion-relaxation correlation (DRCOSY) plot in Figure 9 shows two intensive peaks close to the $T_2 - D$ diagonal and a couple of less intensive peaks at low T_2 values. The diffusion coefficients of the two intensive diagonal peaks correspond well with the fast and slow components of the two-exponential fit of the 13-interval PFG NMR measurements (compare Tab. 1). These results prove that both components with different diffusion coefficients differ also in their T_2 relaxation times. The fast-diffusing benzene molecules relax with a higher and the slow diffusing benzene molecules with a lower T_2 value. For liquid-like molecular mobilities, a lower T_2 value indicates a smaller molecular mobility. Hence, the measured diffusion-relaxation correlation shows that a reduced translational mobility of the benzene molecules (measured in the diffusion dimension of Fig. 9) is accompanied by a reduced local mobility (measured in the relaxation dimension).

The question arises, which of the two components (D_A and D_B) can be assigned to intracrystalline diffusion in the undisturbed pore network of MOF-5. It is known that the MOF-5 frameworks may form interpenetrated crystal structures [37]. Our own MD simulation of self-diffusion in such interpenetrated MOF-5 structures reveals that benzene is immobilized in such cases. This is not observed in the NMR diffusion studies, which show that also the slow diffusing component has a much higher mobility than predicted by MD simulation for an interpenetrated MOF-5 network. This is in agreement with the observed X-ray powder diffraction data presented in Section 3.1.3, which do not indicate the presence of interpenetrated structures in our MOF-5 samples.

However, residual solvent (DEF) molecules as evidenced in the solid-state NMR spectra (Fig. 6) may
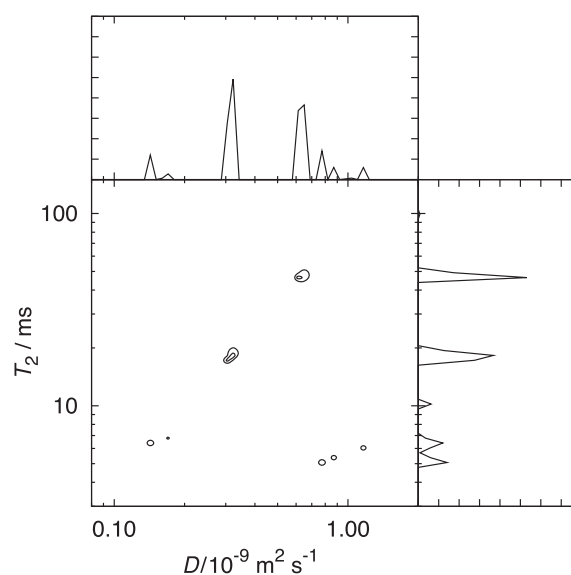

Fig. 9. Two-dimensional diffusion-relaxation correlation (DR-COSY) spectrum of benzene adsorbed at MOF-5 (32Bz) at $\Delta = 20\,\mathrm{ms}$.

interact with the adsorbed benzene molecules and, thus, reduce the local and translational mobilities. Since the two correlation peaks in Figure 9 are sharp and since there is no time dependence of the spin-echo attenuation, there is obviously no fast diffusional exchange between the two domains of different benzene mobilities during the time scales of the NMR experiments. This means that the regions, where the self-diffusion is hindered and the T_2 relaxation time is reduced by DEF molecules, must be well separated from such regions where there are no such interactions. The extension of these regions in the MOF-5 crystal volume must be larger than the mean displacement of the benzene molecules during the time scale of the NMR experiment, which is of the order of 10^{-5} m.

Thus, bringing all the arguments together, it might be possible that the residual DEF molecules only remain in center parts of the MOF-5 crystals, while – due to the successive washing of the crystal with DMF, chloroform and benzene – the outer regions are solvent free. We conclude that the fast component (about 70% of the total amount of adsorbed benzene) represents the intracrystalline self-diffusion coefficient inside an undisturbed lattice of MOF-5, while the component with slower self-diffusion is caused by diffusion in MOF-5 crystal regions where residual DEF molecules hinder the molecular mobility. Therefore, we only discuss the diffusion behavior of the fast component in the following.

Figure 10 compares the experimentally determined self-diffusion coefficients for different loadings and temperatures (fast component) with data obtained by MD simulations [13]. For low loadings of 6 and 10 benzene molecules per unit cell and a temperature of 298 K, there is an agreement between the results obtained by both methods. Above 10 molecules per unit cell, the NMR data show a sharp drop, while the MD data first peak at about
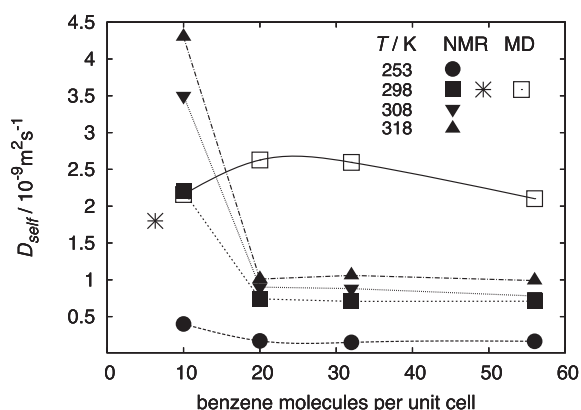
Fig. 10. Loading dependence of the self-diffusion coefficients obtained by PFG NMR ($\blacktriangledown$, $\blacktriangle$, $\blacksquare$, $\bullet$ this work; $\ast$ [26]) inside MOF-5 at various temperatures and comparison to the data obtained by MD simulations at $T = 298$ K ($\square$ [13]). For small loadings NMR and MD data agree within the experimental uncertainty. For loadings exceeding 10 molecules per unit cell the NMR data exhibit a pronounced drop and are found to be a factor of 3 lower than the data obtained by MD simulations.

Fig. 11. Temperature dependence of the self-diffusion of the fast-diffusing benzene component in MOF-5 for different loadings. The activation energies of the self-diffusion are $E_A = 26.5$ kJ mol^{-1} at a loading of 10 molecules per unit cell (10Bz, $\blacksquare$) and about $E_A = 16.1$ kJ mol^{-1} for the higher loadings.

20–30 molecules per unit cell and then decrease slightly for the highest loading of 56 molecules per unit cell. In this region of high loadings, the data obtained by MD simulations exceed the experimental NMR data by about a factor of 3.

Figure 11 shows the temperature dependence of the fast component of the intracrystalline self-diffusion of benzene in MOF-5. Its slope yields the activation energy of self-diffusion. At low loadings, the activation energy is found to be $E_A = (26.5 \pm 3.0)$ kJ mol^{-1}. This is a factor of 2 larger than recently published results of MD simulations ((13.8 ± 1.3) kJ mol^{-1}) [13]. At loadings, which exceed 10 molecules per unit cell, the experimental activation energy is found to be $E_A = (16.1 \pm 2.0)$ kJ mol^{-1}. Simultaneously, the pre-exponential factor D_0 (compare Eq. (1)) drops significantly for loadings exceeding 10 molecules per unit cell.

The agreement between the experimental NMR data and the results obtained by MD simulations at low loadings (6 and 10 molecules per unit cell, 298 K) shows that the main interactions between the MOF-5 framework and the diffusing benzene molecules are well represented in the MD simulation model. The discrepancies between the NMR and MD data at higher loadings are unexpected and not yet understood. Additionally, the activation energies obtained by both methods in the low loading regime differ significantly by $\Delta E_A = 13$ kJ mol^{-1}.

From the experimental point of view, the accuracy of the NMR diffusion measurements even improves for higher loadings due to an increased NMR signal-to-noise ratio compared to the lower loadings. Since there is also no diffusion time dependence of the measured diffusivities, the NMR data are found to be self-consistent for different measurement conditions. It has to be concluded that the observed drop of the self-diffusion coefficient at about 20 molecules per unit cell is not an artifact of the experiment. If – in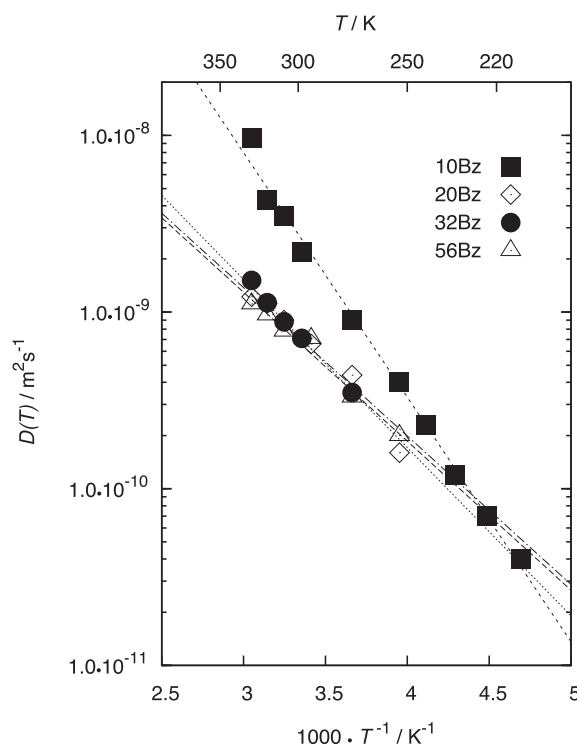 the high loading regime – the benzene molecules obviously move slower than predicted by MD simulation data, the observed drop of mobility points toward additional interactions which become important at higher loadings and which are not yet included in the MD simulation model.

In the MD simulations periodic boundary conditions are used to approximate the ideal crystalline environment and additional remaining solvent molecules like DEF are usually not considered. The benzene-DEF interactions are mainly leading to the diffusion component of slower mobility (see Tab. 1), which is not considered in this comparison between NMR and MD data. Additional attractive benzene-benzene dispersion forces could mean that several molecules tend to cluster. Using Monte Carlo and MD simulations, Krishna and van Baten [15] discussed recently the formation of clusters of small adsorbed molecules in several microporous materials at subcritical temperatures. In the case of carbon dioxide in MOF-5, the authors found that CO_2 clusters form in the pore space at $T = 200$ K already at relatively small concentrations. This clustering is associated with a pronounced drop of the Fickian diffusivity. Close to the CO_2 critical temperature, no such clustering and an almost concentration independent Fickian diffusivity was predicted for concentrations below 30% pore filling. For more details, see Figures 15a and 15b in reference [15].

Such a clustering, which could be seen as the onset of capillary condensation, means a trading of entropy for

interaction enthalpy for the benzene guest molecules and could be due to the spatial restrictions in the MOF-5 pores. In the theoretical simulations, high temperature MD runs were used to generate non-correlated initial structures for the sampling of the phase space. This, and the restriction to a single unit cell as the simulation domain, might have led to a sampling of the non-clustered phase space only. We are currently performing longer simulations and larger supercells in order to investigate the interactions of benzene in MOF-5 at higher loadings and their impact on mobility.

Since all NMR measurements were performed well below the critical temperature of benzene ($T_c = 562 \, \mathrm{K}$ [40]), clustering of benzene in the MOF-5 pore space might be possible as well. Comparison with the concentration-dependent self-diffusion data in Figure 10 shows that preferential benzene-benzene interactions might occur in the range of 10–20 molecules per unit cell. Sixteen molecules per unit cell correspond to two molecules per A and B cell. Thus, even if we assume a homogeneous benzene distribution, the averaged benzene concentration at 20 molecules per unit cell is high enough to form benzene clusters in the micropores.

It is obvious that it is more difficult for a cluster of benzene molecules to move through the pore network than for single benzene molecules. This leads to the decreased pre-exponential factors at high loadings compared to the low loadings (see Arrhenius plot of the self-diffusion coefficients in Fig. 11). Simultaneously – compared to a single benzene molecule – the cluster of benzene molecules is not able to explore the deepest parts of the potential landscape provided by the MOF-5 lattice. This could lead to the observed smaller activation energy of self-diffusion in the case of higher benzene loadings.

We are aware that these explanations of the observed concentration and temperature dependence of benzene self-diffusion in MOF-5 represent just a preliminary empirical discussion. As described above, MD simulations accounting better for benzene-benzene interaction in metal-organic frameworks are currently set up in our laboratory. Nevertheless, to the best of our knowledge, the experimental observations demonstrate the influence of clustering on self-diffusion of adsorbate molecules in microporous materials and are a further hint that clustering effects are in fact influencing diffusion mechanisms in MOF-5 as predicted in reference [15].

5 Conclusions

In this contribution NMR experiments for the investigations of the mobility of benzene molecules adsorbed in MOF-5 are presented and compared to current data available from MD simulations. The diffusion measurements using the 13-interval PFG NMR pulse sequence and the DRCOSY sequence show that benzene is adsorbed in MOF-5 in two domains with different mobilities. X-ray powder diffraction indicates that the crystal structure of the MOF-5 samples does not show significant crystal defects, which might reduce the mobility of a fraction of the adsorbed benzene molecules. By ^{1}H MAS NMR residual solvent molecules (DEF) were detected. We assume that they are located in the central parts of the large crystals, where they could not be removed from by washing after synthesis. There they block partially diffusion pathways leading to the fraction of the adsorbed benzene molecules with lower mobility.

The benzene molecules with the higher mobility are adsorbed in the undisturbed MOF-5 lattice and are therefore compared to the data obtained in the MD simulation. The experimentally observed steep decrease of mobility from low loadings (10 molecules per unit cell) to higher loadings (20 molecules per unit cell) is not reproduced in the MD simulations. It is probably caused by intermolecular forces between benzene molecules, which lead to clustering. Such information about self-diffusion in the high loading regime was not available before and might help to improve future MD simulations.

References

1. O.M. Yaghi, G. Li, T.L. Groy, J. Solid State Chem. **117**, 256 (1995)
2. M. Eddaoudi, J. Kim, N. Rosi, D. Vodak, J. Wachter, M. O'Keeffe, O.M. Yaghi, Science **295**, 469 (2002)
3. J.L.C. Rowsell, O.M. Yaghi, Microporous Mesoporous Mater. **73**, 3 (2004)
4. S. Shimomura, S. Horike, S. Kitagawa, Chemistry and application of porous coordination polymers, in *Proc. of 15th Int. Zeolite Conf.*, edited by J.C. Ruren Xu, Z. Gao, W. Yan, vol. 170, *Studies in Surface Science and Catalysis* (Elsevier, Amsterdam, 2007), pp. 1983–1990
5. G. Férey, C. Mellot-Draznieks, C. Serre, F. Millange, J. Dutour, S. Surble, I. Margiolaki, Science **309**, 2040 (2005)
6. U. Mueller, M. Schubert, F. Teich, H. Puetter, K. Schierle-Arndt, J. Pastré, J. Mater. Chem. **16**, 626 (2006)
7. S. Keskin, D.S. Sholl, Langmuir **25**, 11786 (2009)
8. E. Haldoupis, S. Nair, D.S. Sholl, J. Am. Chem. Soc. **132**, 7528 (2010)
9. S. Kaskel, F. Schüth, M. Stöcker, Microporous Mesoporous Mater. **73**, 1 (2004)
10. S. Kaskel, Chem. Ing. Tech. **82**, 1019 (2010)
11. J. Juan-Alcañiz, E.V. Ramos-Fernandez, U. Lafont, J. Gascon, F. Kapteijn, J. Catal. **269**, 229 (2010)
12. A. Skoulidas, D.S. Sholl, J. Phys. Chem. B **109**, 15760 (2005)
13. S. Amirjalayer, M. Tafipolsky, R. Schmid, Angew. Chem. Int. Edit. **46**, 463 (2007)
14. C. Xue, Z. Zhou, B. Liu, Q. Yang, C. Zhong, Mol. Simul. **35**, 373 (2009)
15. R. Krishna, J.M. van Baten, Langmuir **26**, 3981 (2010)
16. L. Heinke, J. Kaerger, New J. Phys. **10**, 1 (2008)

17. C. Chmelik, J. Kaerger, M. Wiebcke, J. Caro, J.M. van Baten, R. Krishna, Microporous Mesoporous Mater. **117**, 22 (2009)
18. C. Chmelik, H. Bux, J. Caro, L. Heinke, F. Hibbe, T. Titze, J. Kaerger, Phys. Rev. Lett. **104**, 085902-1 (2010)
19. N. Rosenbach Jr., H. Jobic, A. Ghoufi, F. Salles, G. Maurin, S. Bourrelly, P.L. Llewellyn, T. Devic, C. Serre, G. Ferey, Angew. Chem. Int. Edit. **47**, 6611 (2008)
20. F. Salles, D.I. Kolokolov, H. Jobic, G. Maurin, P.L. Llewellyn, T. Devic, C. Serre, G. Ferey, J. Phys. Chem. C **113**, 7802 (2009)
21. F. Salles, H. Jobic, T. Devic, P.L. Llewellyn, C. Serre, G. Ferey, G. Maurin, Am. Chem. Soc. Nano **4**, 143 (2010)
22. F. Stallmach, P. Galvosas, in *Annu. Rep. NMR Spectrosc. Review*, vol. 61 (Elsevier, 2007) pp. 51–131
23. M. Wehring, J. Gascon, D. Dubbeldam, F. Kapteijn, R.Q. Snurr, F. Stallmach, J. Phys. Chem. C **114**, 10527 (2010)
24. P. Callaghan, S. Godefroy, B. Ryland, J. Magn. Reson. **162**, 320 (2003)
25. D. Pérez, A. Benavides, M. Martín-Landrove, Eur. Phys. J. Appl. Phys. **42**, 321 (2008)
26. F. Stallmach, S. Gröger, V. Künzel, J. Kärger, O.M. Yaghi, M. Hesse, U. Müller, Angew. Chem. Int. Edit. **45**, 2123 (2006)
27. S. Amirjalayer, R. Schmid, Microporous Mesoporous Mater. **125**, 90 (2009)
28. H. Li, M. Eddaoudi, M. O'Keeffe, O.M. Yaghi, Nature **402**, 276 (1999)
29. H. Karge, J. Weitkamp (eds.), *Molecular Sieves – Adsorption and Diffusion* (Springer-Verlag, Berlin, Heidelberg, 2008), p. 105
30. E.O. Stejskal, J.E. Tanner, J. Chem. Phys. **42**, 288 (1965)
31. J.E. Tanner, J. Chem. Phys. **52**, 2523 (1970)
32. E.L. Hahn, Phys. Rev. **80**, 580 (1950)
33. R.R. Valiullin, V.D. Skirda, S. Stapf, R. Kimmich, Phys. Rev. E **55**, 2664 (1997)
34. R. Cotts, M. Hoch, T. Sun, J. Markert, J. Magn. Reson. **83**, 252 (1989)
35. L. Venkataramanan, Y.Q. Song, M.D. Hürlimann, IEEE Trans. Signal Process. **50**, 1017 (2002)
36. Y.Q. Song, L. Venkataramanan, M.D. Hürlimann, M. Flaum, P. Frulla, C. Straley, J. Magn. Reson. **154**, 261 (2002)
37. J. Hafizovic, M. Bjorgen, U. Olsbye, P.D.C. Dietzel, S. Bordiga, C. Prestipino, C. Lamberti, K.P. Lillerud, J. Am. Chem. Soc. **129**, 3612 (2007)
38. T. Loiseau, H. Muguerra, G. Férey, M. Haouas, F. Taulelle, J. Solid State Chem. **178**, 621 (2005)
39. P. Galvosas, F. Stallmach, G. Seiffert, J. Kärger, U. Kaess, G. Majer, J. Magn. Reson. **151**, 260 (2001)
40. D.R. Lide (ed.), *CRC Handbook of Chemistry and Physics*, 87th edn. (CRC Press, Boca Raton, FL, 2006)